Multicomponent alloys with thermally, mechanically and magnetically controlled shape memory effects

Journal of Physics: Conference Series **1389** (2019) 012098 doi:10.1088/1742-6596/1389/1/012098

Multicomponent alloys with thermally, mechanically and magnetically controlled shape memory effects

A V Okulov[1], E S Belosludtseva[1], N N Kuranova[1,2], E B Marchenkova[1], A V Pushin[1,2] and V G Pushin[1,2]

[1]M.N. Miheev Institute of Metal Physics of UD of RAS, 620108 Ekaterinburg, S. Kovalevskaya, 18, Russia
[2]Ural Federal University Named after the First President of Russia B.N. Yeltsin, 620002 Ekaterinburg, Mira, 19, Russia

E-mail: okulovartem@imp.uran.ru

Abstract. This paper presents a brief review of the systematic study of the influence of the chemical composition on the structure, phase transformations and physical properties of binary and quasi-binary Ti-Ni, TiNi-TiFe, TiNi-NiCu, NiMn-NiGa and Ni_2MnGa-Ni_3Ga systems, which undergo thermoelastic martensitic transformations (TMT) and related with them thermally, mechanically, or magnetically controlled shape memory effects (SME). The effect of alloying with a third component on the behavior of critical temperatures and the TMT sequence has been established, and their generalized diagrams have been constructed. It is shown that the morphology of thermoelastic martensite is a hierarchy of packets of thin coherent crystals.

1. Introduction

Smart alloys, which undergo highly reversible thermo-, mechano-, and magnetoelastic martensitic phase transformations, have been of great interest to scientists for a number of years. Due to the intrinsic characteristics of these alloys, such as the shape-memory effect (SME) and giant mechanical pseudo-elasticity effect (PEE) (tens percents), they are promising innovative materials for various technical and medical applications. Among a great number of such alloys, atomically ordered compositions based on TiNi and Ni_2MnGa (Heusler alloys) intermetallics are of particular importance [1–6]. As is known, binary TiNi-based compositions exhibit the best combination of physico-mechanical characteristics among shape-memory alloys. The unique peculiarity of ferromagnetic Heusler alloys is the possibility to control the thermomagnetic transformation (TMT), SME, and PEE by using not only temperature variations and external mechanical forces (for example, for TiNi-based alloys) but also an applied magnetic field [3]. There is a great demand in modern science and technology for new and advanced materials operating under different conditions, particularly new shape-memory alloys. The use of complex alloying and various new breakthrough high-tech methods for the synthesis of metallic materials has become increasingly important. To prepare alloys with high temperature TMT and SME, compositions based on the $Ti_{50}Ni_{50}$ and $Ni_{50}Mn_{50}$ stoichiometric compound can be used; to prepare materials with record magnetoelastic effects, alloys with the ferromagnetic austenite based of the $Ni_{50}Mn_{25}Ga_{25}$ stoichiometric compound can be used. The present work reviews the study of structural and magnetic phase transformations and properties of alloys prepared by mutual alloying of binary and quasi-binary $Ti_{49}Ni_{51}$, $Ti_{49.5}Ni_{50.5}$, $Ti_{50}Ni_{49}Fe_1$, $Ti_{50}Ni_{47}Fe_3$,

$Ti_{50}Ni_{40}Cu_{10}$, $Ti_{50}Ni_{38}Cu_{10}Fe_2$, $Ti_{50}Ni_{50}$–$Ti_{50}Fe_{50}$, $Ti_{50}Ni_{50}$–$Ni_{50}Cu_{50}$, $Ni_{50}Mn_{50}$–$Ni_{50}Ga_{50}$ and $Ni_{75}Ga_{25}$–$Ni_{50}Mn_{25}Ga_{25}$ systems. The studies performed in recent years at the Institute of Metal Physics, Ural Branch, Russian Academy of Sciences, are given particular attention.

2. TiNi-based alloys

In this work, the main task was to obtain TiNi-based alloys as close in composition as possible to stoichiometry (tables 1, 2). The X-ray phase analysis showed that all the alloys are predominantly in the *B*2 austenitic state at room temperature. According to low-temperature X-ray diffraction data, the phase composition was established and the parameters of *B*2 austenite and martensite of the alloys were measured [4].

As a rule, for measuring the critical temperatures of the start (M_s, M'_s) and finish (M_f, M'_f,) of the forward and the start (A_s, A'_s) and finish (A_f, A'_f) of the reverse TMT of TiNi-based alloys are most often used the electrical resistance ρ(T). We carried out measurements of the ρ(T) curves in the thermal cycles «cooling – heating – cooling» for all the studied alloys, on which the temperature «loops» ρ(T) are clearly identified, corresponding to the temperature hysteresis of the TMT (figure 1). The critical temperatures of TMT were determined from ρ(T) using the two-tangent method. They are listed in tables 1 and 2 [4].

Table 1. The critical temperatures of the forward TMT in TiNi-based alloys [4].

Compounds	TMT sequence	M_s, *K*	M_f, *K*	M'_s, *K*	M'_f, *K*
$Ti_{49}Ni_{51}$	B2–B19'–B2	195	150		
$Ti_{49.5}Ni_{50.5}$	B2–R–B19'–B2	300	270	270	210
$Ti_{50}Ni_{49}Fe_1$	B2–R–B19'–B2	310	290	280	245
$Ti_{50}Ni_{47}Fe_3$	B2–R–B19'–R–B2	270	250	150	120
$Ti_{50}Ni_{40}Cu_{10}$	B2–B19–B19'–B19–B2	330	300	230	150
$Ti_{50}Ni_{38}Cu_{10}Fe_2$	B2–B19–B19'–B19–B2	250	230	150	105

Table 2. The critical temperatures of the reverse TMT in TiNi-based alloys [4].

Compounds	TMT sequence	A_s, *K*	A_f, *K*	A'_s, *K*	A'_f, *K*
$Ti_{49}Ni_{51}$	B2–B19'–B2	210	220		
$Ti_{49.5}Ni_{50.5}$	B2–R–B19'–B2	320	325		
$Ti_{50}Ni_{49}Fe_1$	B2–R–B19'–B2	260	320		
$Ti_{50}Ni_{47}Fe_3$	B2–R–B19'–R–B2	190	215	255	280
$Ti_{50}Ni_{40}Cu_{10}$	B2–B19–B19'–B19–B2	185	235	310	345
$Ti_{50}Ni_{38}Cu_{10}Fe_2$	B2–B19–B19'–B19–B2	120	175	250	270

The analysis showed that with increasing Ni content close to the stoichiometric composition or when alloying with Fe (1 and 3 at. %), Cu (10 at. %), or Cu (10 at. %) and Fe (2 at. %), all temperatures of TMT are reduced with different extent depending on the content of alloying additives. The critical temperatures of the TMT were compared for the same types of sequences B2–R–B19' and B2–B19–B19'. For example, when alloyed with Fe the critical temperatures decrease [4].

In this case, the TMT sequence becomes more complicated: alloying with Fe causes the formation of intermediate *R*-martensite, and alloying with Cu, on the contrary, – intermediate *B*19 martensite. It is noteworthy that additional alloying of $Ti_{50}Ni_{40}Cu_{10}$ alloy with Fe led only to a proportional decrease in critical temperatures without changing the TMT sequence [4].

The measurements of the elastic moduli on single crystals showed that all studied TiNi-based alloys experience a pronounced pre-martensitic quasi-isotropic softening of the *B*2 austenite crystal lattice, in which all independent modules C_{11}, C_{12}, C_{44}, and $C'=(C_{11}-C_{12})/2$ experience almost the same decrease when approaching the intercritical temperature range (ITR) of TMT (figure 2) according to [4].

The electron microscopic study of the microstructure of quasi-binary alloys has shown the presence of a predominantly packet morphology of pairwise twinned martensitic crystals (figures 3–5). At the same time, the presence of thin secondary twins of type I along various shear systems is tipical for the

R, *B*19, and *B*19' martensites, they are practically parallel to the soft shear system {011}<01$\bar{1}$> in *B*2 austenite, individual for each martensite (for *R* along {101} and {100} planes, for *B*19 and *B*19' along (111) or (011) planes). The peculiarity of the internal structure of *B*19' crystals is in the presence of thin secondary composite nanotwins and stacking faults along the $(001)_{B19'}$ (figures 3 and 5). Different morphological variants of B19'and R martensite crystals are shown in figures 3 and 4, respectively [4].

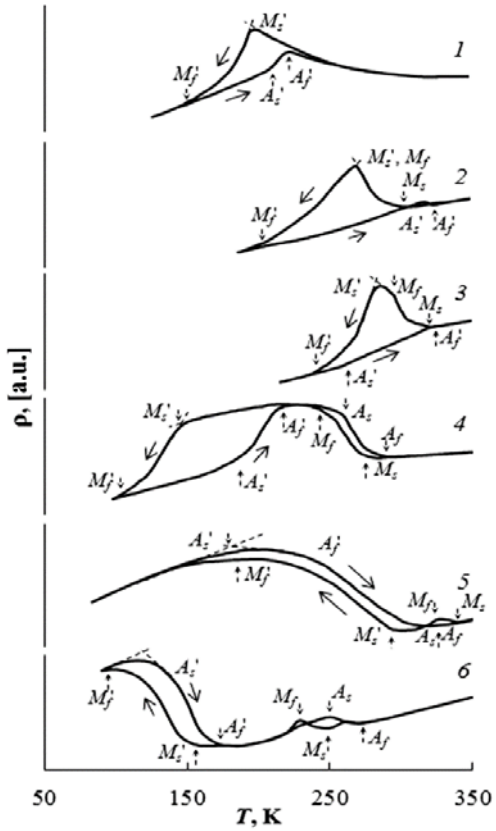

Figure 1. Temperature dependences of the electrical resistance of alloys $Ti_{49}Ni_{51}$ (curve 1), $Ti_{49.5}Ni_{50.5}$ (curve 2), $Ti_{50}Ni_{49}Fe_1$ (curve 3), $Ti_{50}Ni_{47}Fe_3$ (curve 4), $Ti_{50}Ni_{40}Cu_{10}$ (curve 5), $Ti_{50}Ni_{38}Cu_{10}Fe_2$ (curve 6) [4].

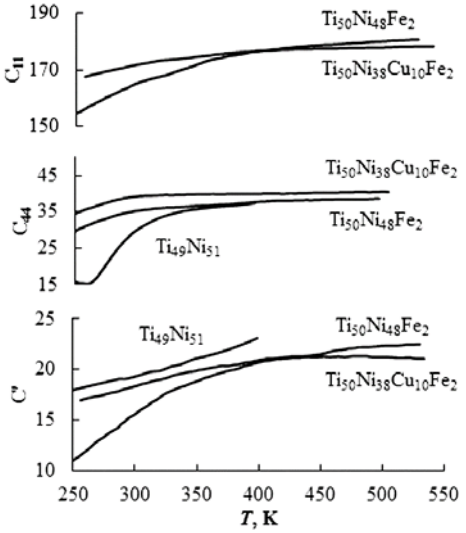

Figure 2. Temperature dependences of the elastic moduli (GPa) [4].

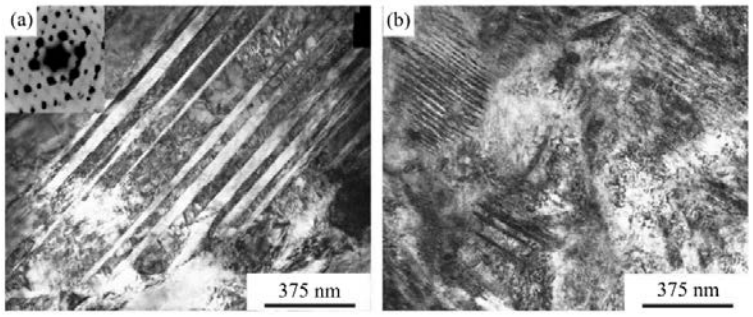

Figure 3. TEM images of *B*19'-martensite alloy $Ti_{50}Ni_{50}$ and microelectron diffraction pattern (inset) [4].

In this case, the electron diffraction patterns correspond to sharp drawing rods in the directions of the reciprocal lattice along the $[001]_{B19'}$. Nanotwins of type $(001)_{B19'}$, which are located at an angle to

the boundaries of twins in packets, are also detected, for example, in the dark field image (figure 5, d). The unique peculiarity of the internal structure of *R* and *B*19 martensite crystals is the presence of antiphase domains along their boundaries visualized in figures 4, b and 5, c. It is obvious that such a high defectiveness of the fine structure, formed during the TMT, causes an increase in the electrical resistance in the ITR [4].

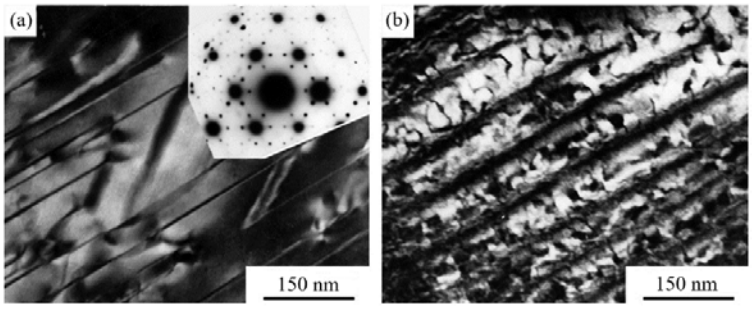

Figure 4. TEM images of $Ti_{50}Ni_{47}Fe_3$ *R*-martensite and microelectron diffraction pattern (inset) [4].

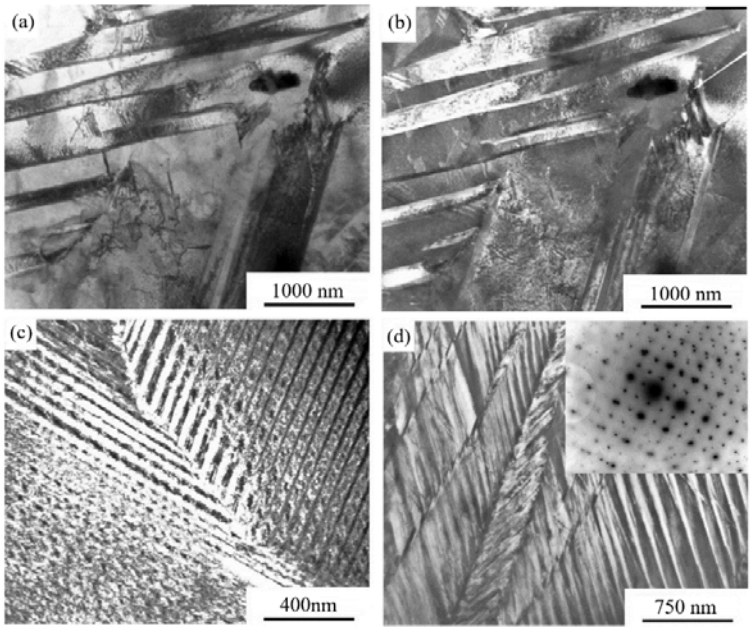

Figure 5. TEM images of $Ti_{50}Ni_{40}Cu_{10}$ (a) in the bright field and (b) in the dark field and (c, d) $Ti_{50}Ni_{38}Cu_{10}Fe_2$; (a–c) *B*19-martensite and (d) *B*19’-martensite and microelectron diffraction pattern (inset) [4].

3. Heusler alloys

In this work, we constructed generalized diagrams of phase transformations in Ni_2MnGa-based alloys (figure 6) using obtained experimental results and available literature data. The fact that the martensitic transformation in the $Ni_{50}Mn_{50}$ stoichiometric alloys occurs in the range of high critical temperatures of the onset, M_s = 970 K, and end of both forward, M_f = 920 K, and reverse transformations during heating, A_s = 970 K, A_f = 1020 K drew much attention. In this case, the ITR (A_f –M_f) does not exceed 100 K. According to figure 6, the alloying with Ga, firstly, reduces all critical temperatures and ITR and, secondly, leads to temperature hysteresis of TMT. The narrow temperature hysteresis ΔT (less than 50 K) is typical of the thermoelastic nature and specific mechanisms of TMT responsible for the SME in metastable low-modulus intermetallic alloys [2, 3, 5, 6].

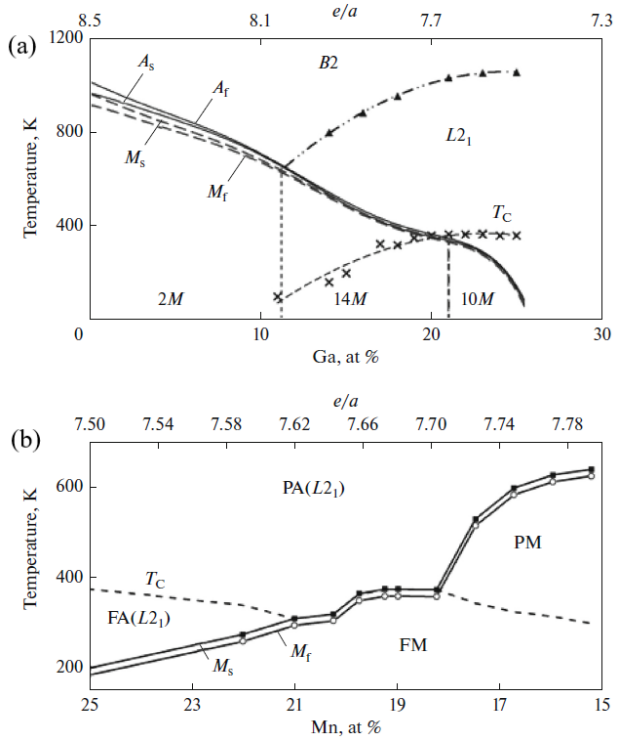

Figure 6. Phase transformation diagrams for the (a) $Ni_{50}Mn_{50-z}Ga_z$ and (b) $Ni_{50}Mn_{25}Ga_{25}$–$Ni_{60}Mn_{15}Ga_{25}$ systems [5].

The phase composition of all the studied alloys has been accurately determined (figure 6). The crystal lattice type of both austenite (*B*2, $L2_1$) and martensite (2*M*, 10*M*, 14*M*) depends on the chemical composition and average electron concentration of alloys. For example, at room temperature, the martensite of the $Ni_{50}Mn_{50}$ alloyed with 11–12 at. % Ga is ordered with the formation of the tetragonal $L1_0$ (2*M*) structure. X-ray and electron diffraction patterns of the other alloys demonstrate diffraction reflections belonging to long-period martensite phases (10*M* and 14*M*), variations of the lattice parameter of which indicate the role of atomic size factor. The $L2_1 \leftrightarrow 10M$ TMT in the alloys with a Ga content (22–25 at. %) occurred at temperatures below room temperature. The lattice parameters of the 14*M* martensite in the alloys with 11–21 at. % Ga are $a = 0.423$, $b = 0.550$, $c = 2.935$ nm, $\beta = 92.90°$. Meanwhile, the structural and magnetic transition behavior of the alloys with different e/a and Mn (at. %) contents divide the structural-magnetic phase diagram (figure 6, b) into four regions representing different crystallographic and magnetic states of the alloys: ferromagnetic austenite (FA), paramagnetic austenite (PA), ferromagnetic martensite (FM), and paramagnetic martensite (PM) [5].

In coarse grains, packets are jointed along packet boundaries, which can be both planar and stepped twisting, although they were separated by coherently jointed twinned crystals, which almost coincide with magnetic domains (figure 7). The martensite in the studied alloys are packet pyramidal morphology and consists of finely twinned crystals. In small grains (to 5 μm in size), as a rule, we observed a single packet of martensite plates (figure 8).

Figure 8 shows typical images of the microstructures of 2*M* and 14*M* martensite and direct atomic resolution imaging the 14*M* martensite lattice. Electron diffraction patterns exhibit twin-type reflections and extra reflections spaced 1/5 and 1/7 apart between fundamental Bragg reflections, which correspond to the 10*M* and 14*M* phase, respectively (figure 8). The combined trace analysis of electron micrographs and electron diffraction patterns allowed us to show that martensite consists of packets of pairwise twinned parallel lamellae with the habitus plane close to $\{011\}B2/L2_1$ and thin secondary internal twins along one of the 24 equivalent «soft» $\{011\}<01\bar{1}>$ $B2/L2_1$ twinning shear systems [2, 3, 5, 6].

The presence of a hierarchy of twinned crystal packets in the alloys results from the action of a multinucleus thermomagnetic transformation mechanism and subsequent accommodation twinning, which can develop as martensite cools down. The main cause for the formation of a well organized hierarchy of coherent twin crystals in the low-module alloys is likely the anisotropic elastic stresses that are accommodatively accumulated in the course of such thermoelastic martensitic transformations. The thermoelastic mechanism of the transformation determines a very low dislocation concentration in the crystals of 2*M*, 10*M* and 14*M* martensite phases, recurrence of their micromorphology upon thermal cycling, and, the most important, the presence of SME and PEE [1–7]. For all Ni_2MnGa-based alloys, it was found the dependence of structural type of martensite crystals on the electron concentration, *e*. When the *e/a* in the quasi-binary alloys with Ga is 8.50–8.00, the martensite structure is 2*M*; when 8.00 > *e/a* > 7.70, the martensite structure is 14*M*. At 7.70 ≥ *e/a* ≥ 7.62, the martensite is 10*M* (figure 6) [5].

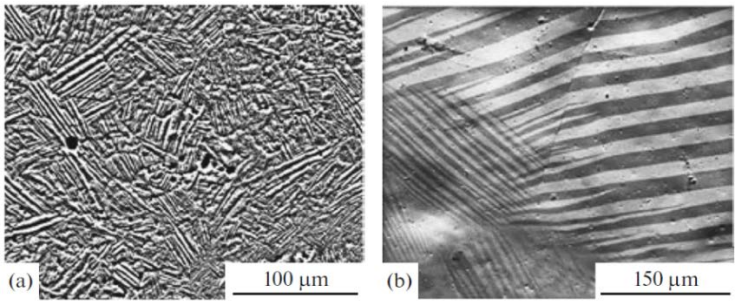

Figure 7. SEM images of the microstructure of the (a) $Ni_{50}Mn_{50}$ and (b) $Ni_{50}Mn_{28}Ga_{22}$ alloys [5].

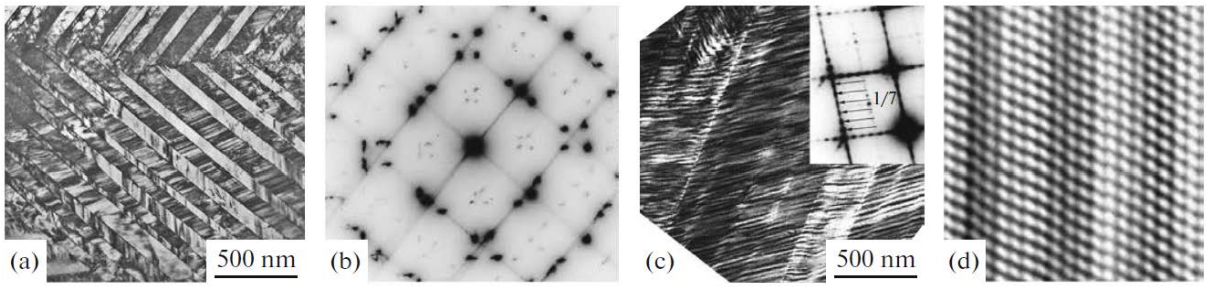

Figure 8. TEM images of the (a) 2*M* and (c) 14*M* martensite, and (b) inset in (c) associated electron diffraction patterns, and (d) direct atomic-resolution imaging the14*M* martensite lattice [5].

4. Conclusion

Thus, the critical temperatures of TMTs in the TiNi- and Ni_2MnGa-based alloys were measured. The peculiarities and differences of the packet microstructure of pairwise twinned martensite crystals of TiNi-based alloys, in which the twinning shear systems are inherited from the soft shear systems {011}<01$\bar{1}$> in *B*2 austenite, are established. The elastic moduli of TiNi-based alloys were measured. Moreover, it was established the behavior of the increase of the electrical resistance in TiNi-based alloys in the ITR. Based on the obtained microstructural data of Ni_2MnGa-based alloys, it was proposed the crystallographic mechanism of the TMT. For all Ni_2MnGa-based alloys, it was found the dependence of structural type of martensite crystals on the electron concentration, *e*.

Acknowledgments

This work was performed within the state task of Federal Agency for Scientific Organizations (theme Struktura, no. AAAA-A18-118020190116-6), with the support of the Project UB RAS (no. 18-10-2-39) and was partly supported by the Russian Foundation for Basic Research (project no. 18-32-00529 mol_a).

References

[1] Otsuka K, Shimizu K, Suzuki Y, Sekiguchi Y, Tadaki C, Honma T and Miyazaki S 1990 *Shape Memory Alloys* ed H Funakubo (Moscow: Metallurgiya)
[2] Pushin V G, Kondrat’ev V V and Khachin V N 1998 *Pre-transition Phenomena and Martensitic Transformations* (Ekaterinburg: UrO RAN) [in Russian]
[3] Vasil’ev N, Buchel’nikov V D, Tagaki T, Khovailo V V and Estrin E I 2003 *Phys. Usp*. **46** 550–588
[4] Kuranova N N, Okulov A V, Pushin A V, Pushin V G and Uksusnikov A N 2015 *Intern. J. Appl. & Fundam. Res.* **12** 422–426 [in Russian]
[5] Pushin V G, Belosludtseva E S and Marchenkova E B 2018 *Phys. Met. Metallogr.* **119** 1191-1195
[6] Belosludtseva E S, Kuranova N N, Marchenkova E B, Popov A G and Pushin V G 2016 *Tech. Phys*. **61** 547–553
[7] Pushin V G 2006 *Titanium Nickelide Alloys with Shape Memory. Part I. Structure, phase transformations and properties* (Ekaterinburg: UrO RAN) 440 [in Russian]